ChemComm

COMMUNICATION

Beyond structure and activity: Targeting Class A Carbapenemase with Monocyclic and Bicyclic Boronic Acids to Counter Antimicrobial Resistance

Accepted 00th January 20xx

DOI: 10.1039/x0xx00000x

Kunal Dhankhar[a, c], Mousumi Hazra[d], Adwaita SR Nair[a, b], Alaa Eddin Alhmedi Alkhatid[a], Narayan C Mishra[c], Saugata Hazra*[a, b]

[a.] *Department of Biosciences and Bioengineering, Indian Institute of Technology, Roorkee, Haridwar, Uttarakhand, INDIA, 247667.*
[b.] *b. Centre for nanotechnology, Indian Institute of Technology, Roorkee, Haridwar, Uttarakhand, INDIA, 247667.*
[c.] *c. Department of Polymer and Process Engineering, Indian Institute of Technology, Roorkee, Haridwar, Uttarakhand, INDIA, 247667.*
[d.] *d. Department of Botany and Microbiology, Gurukula Kangri (Deemed to be University), Haridwar, Uttarakhand, 249404, IN*

Supplementary Information

Table S1. Data collection and refinement parameters for the crystal structures of boronates in complex with SME-1.

Parameters	Vaborbactam	Taniborbactam	Ledaborbactam
PDB ID	9W7N	9W7O	9W7P
Resolution range (Å)	23.76 – 2.00	24.89 – 1.93	21.78 – 2.20
Completeness (%)	99.9	99.9	99.9
Number of observations	217489	279834	180679
Number unique	32253	10854	9716
Final R, R_{free}	0.18, 0.24	0.18, 0.238	0.19, 0.26
Total number of atoms	44986	4621	4327
Total number of water molecules	255	363	165
Space group	P 1 21 1	P 1 21 1	P 1 21 1
Cell constants, a, b, c, α, β, γ	36.04Å, 51.01Å 130.53Å, 90.00◦, 92.80◦, 90.00◦	70.82Å, 51.51Å, 74.70Å, 90.00◦, 113.08◦, 90.00◦	36.39Å, 50.47Å, 130.59Å, 90.00◦, 97.72◦, 90.00◦
Mean((I)/sd(I))	14.7	11.8	8.9
Multiplicity	6.7	6.1	7.5
Half-set correlation	0.996	0.961	0.994
Average *B* factors (Å^2)	14	14	16
Wilson B-factor (Å^2)	9.3	12.8	11.9

Table S2. AST profile of Vaborbactam, Taniborbactam, and Ledaborbactam against SME-1. PV: Plasmid vector pet-(28a), RPV: Recombinant plasmid vector with SME-1 Gene.

Disk Diffusion Assay (mm)				
Antibiotic	**Ampicillin**	**Imipenem**	**Cephalothin**	**Cefotaxime**
E. coli TOP 10 with PV	21	27	21	29
E. Coli Top 10 with RPV	12	18	0	18
Vaborbactam	20	26	17	29
Taniborbactam	19	22	14	27
Ledaborbactam	22	27	18	29
MIC (mcg/ml)				
E. Coli Top 10 with PV	2	0.12	8	0.12
E. Coli Top 10 with RPV	32	8	>128	32
Vaborbactam	4	0.25	8	0.12
Taniborbactam	8	0.5	8	0.25
Ledaborbactam	4	0.12	4	0.12

Table S3. MM-GBSA binding energy calculation for the crystal structure of boronates bound with SME-1.

Boronate	Δ_{vdW}	ΔG_{SOLV}	ΔTOTAL
Vaborbactam	-29.4 ±3.34	39.19 ±7.37	-121.83 ±6.52
Taniborbactam	-29.87 ±2.49	52.89 ± 11.26	-122.67 ± 4.78
Ledaborbactam	-30.81 ± 2.75	42.1 ±4.62	-126.64 ±4.3

*All units are reported in kcal/mol

Table S4. MM-PBSA binding energy calculation for the crystal structure of boronates bound with SME-1.

Boronate	Δ_{vdW}	ΔG_{SOLV}	ΔTOTAL
Vaborbactam	-29.87 ±2.75	68.61 ±9.6	-106.95 ±8.06
Taniborbactam	-29.4 ±2.49	47.88 ± 9.89	-113.15 ±6.32
Ledaborbactam	-30.81 ±2.75	53.58 ±7.02	-115.16 ±5.06

*All units are reported in kcal/mol

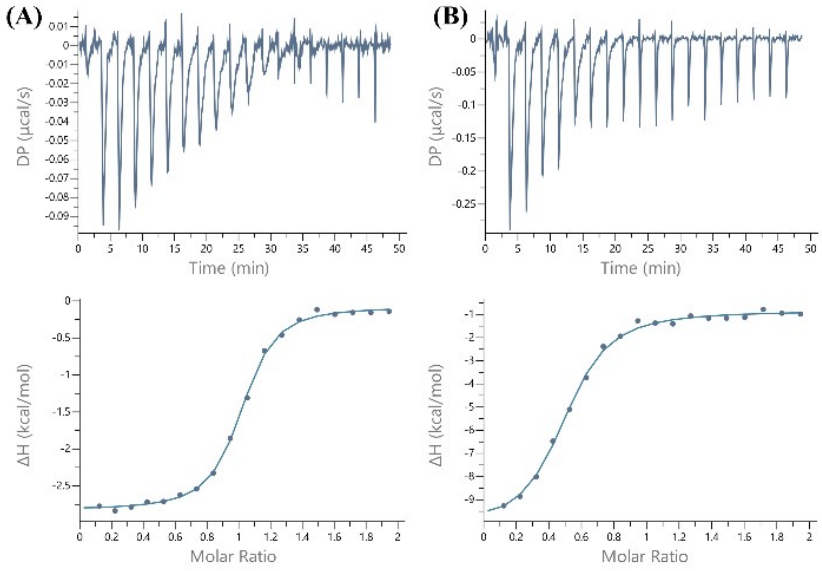

Figure S1: Isothermal Profile of Vaborbactam (A) and Taniborbactam (B).

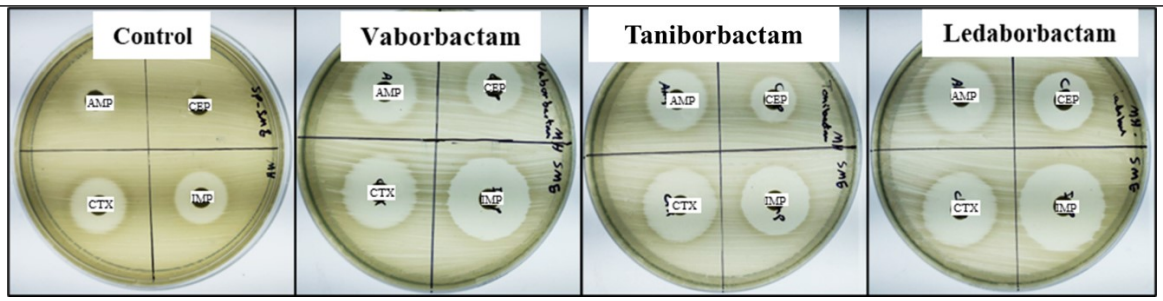

Figure S2: Disk diffusion assay for testing the biological activity of Vaborbactam, Taniborbactam and Ledaborbactam against SME-1 producing *E.coli* TOP10 cells.
AMP: Ampicillin, CEP: Cephalothin, CTX: Cefotaxime, IMP: Imipenem

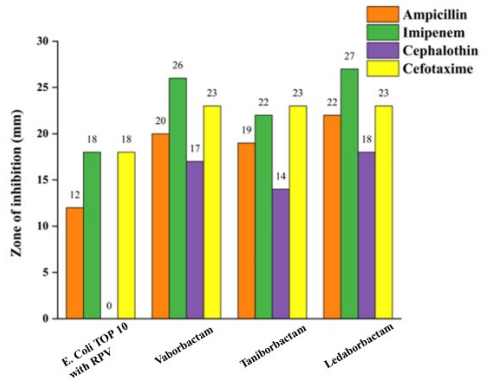

Disk Diffusion Assay (mm)

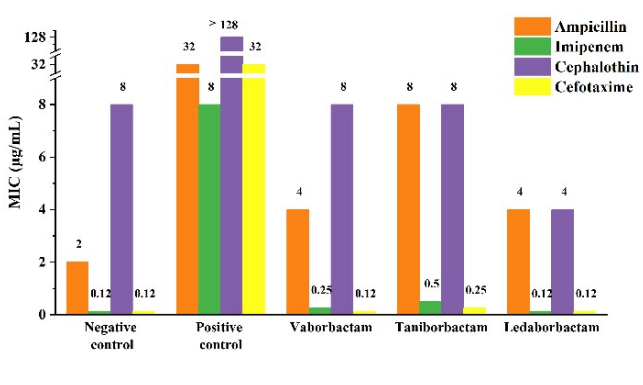

MIC (mcg/ml)

Figure S3: Disk Diffusion and MIC assay of boronates for the biological activity of Vaborbactam, Taniborbactam, and Ledaborbactam against SME-1 producing *E .coli* TOP10 cells. Negative control corresponds to *E. coli* TOP 10 cells with the Plasmid vector without the SME-1 gene. Positive control corresponds to the *E. coli* TOP10 cells with the Recombinant plasmid vector with the SME-1 gene.

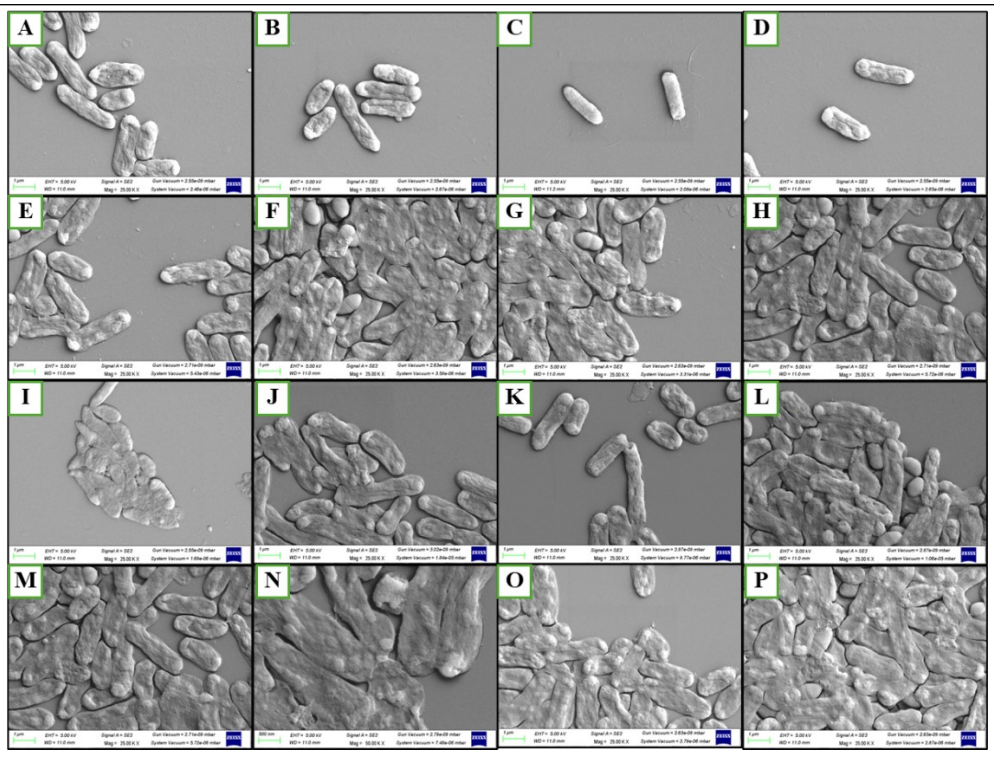

Figure S4: FESEM images of *E.coli* TOP10 producing SME-1 against: Ampicillin (A), Imipenem (B), Cephalothin (C), Cefotaxime, (D), Ampicillin & Vaborbactam (E), Imipenem & Vaborbactam (F), Cephalothin & Vaborbactam (G), Cefotaxime & Vaborbactam (H), Ampicillin & Taniborbactam(I), Imipenem & Taniborbactam(J), Cephalothin & Taniborbactam(K), Cefotaxime & Taniborbactam(L), Ampicillin & Ledaborbactam(M), Imipenem & Ledaborbactam(N), Cephalothin & Ledaborbactam(O), Cefotaxime & Ledaborbactam(P).

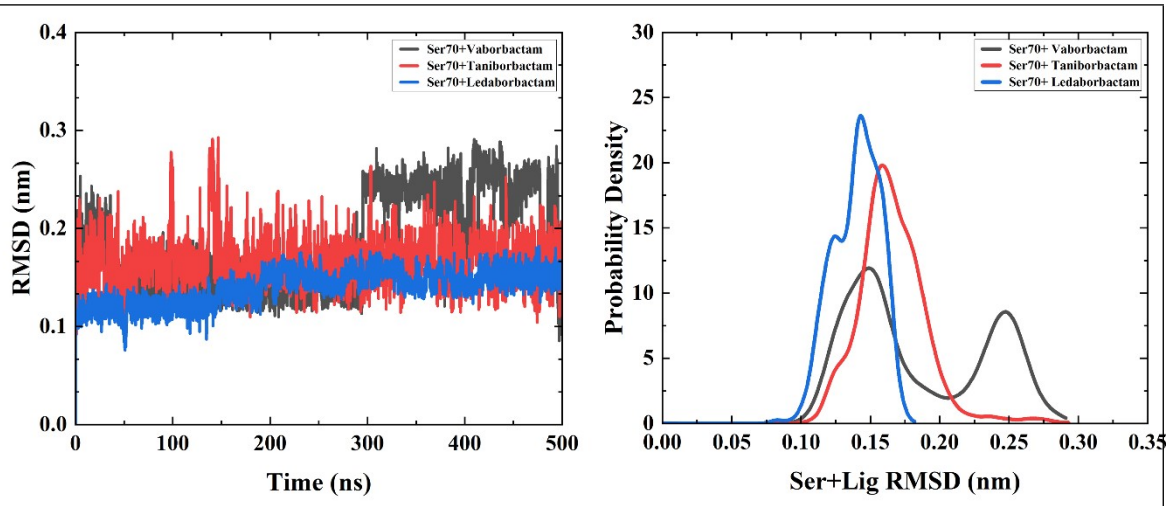

Figure S5. RMSD analysis of the boronic acids bound with SME-1.

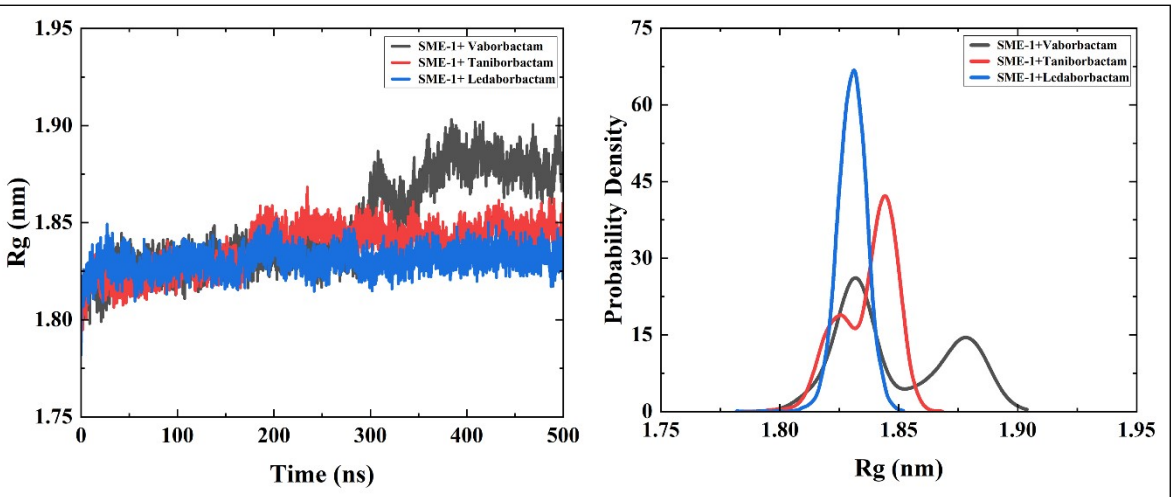

Figure S6. Rg analysis of the boronic acids bound with SME-1.

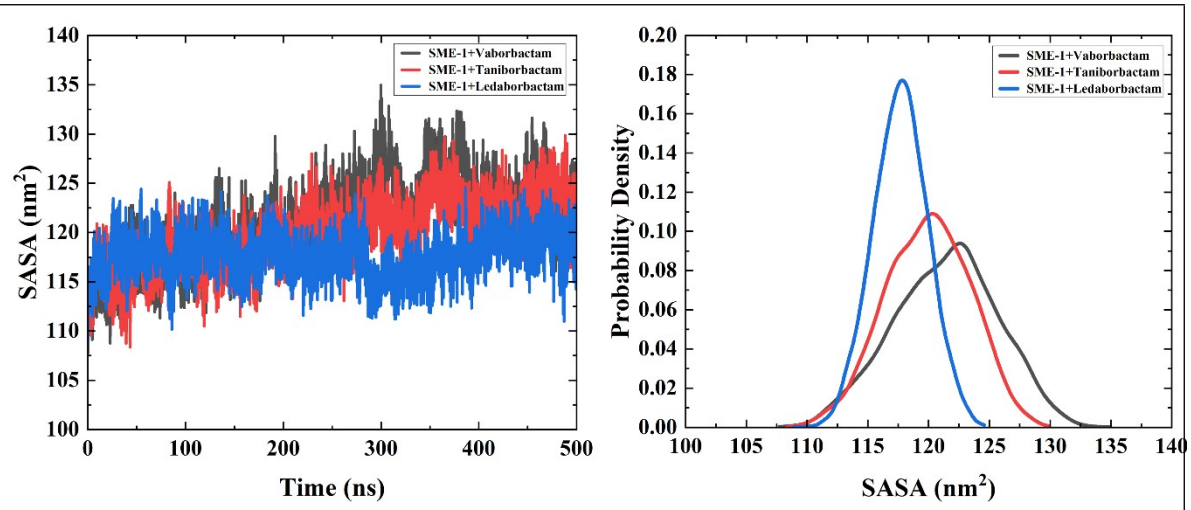

Figure S7. SASA analysis of the boronic acids bound with SME-1.

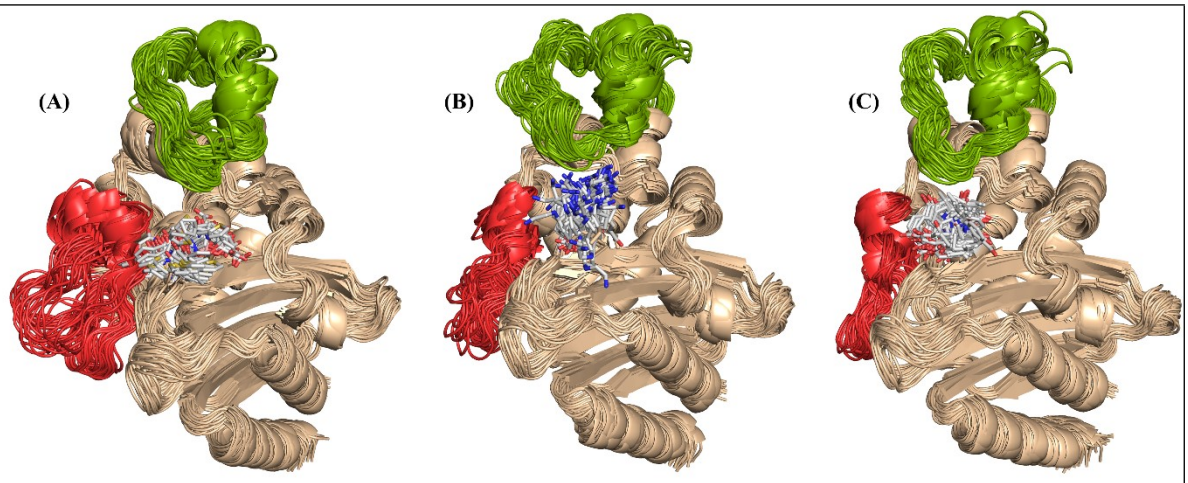

Figure S8. Clustering analysis of the boronic acids bound with SME-1.

Materials and Methods:

Materials: Vaborbactam (RPX7009) was purchased from Cayman Chemical Pvt. Ltd. Taniborbactam (VNRX-5133) and Ledaborbactam (VNRX-5236) were purchased from MedChemExpress Pvt. Ltd.

Cloning, overexpression, & protein purification

SME-1 was expressed and purified as previously described [1]. Briefly, the pET-28a vector was used for cloning of the SME-1 gene from *Serratia marcescens* using NcoI and XhoI as restriction enzymes. Using the heat shock method, the vectors were transformed into competent *E. coli* BL21 (DE3) cells. The overexpression of the protein was analyzed at different IPTG concentrations (0.1-1 mM) and different temperatures (18-25 °C). After optimizing the overexpression condition, the secondary culture media were induced under the same conditions, i.e., 0.5 mM IPTG. After 18 hours of induction, the cells were harvested. These harvested cells were resuspended in 55 mM Tris-HCl (pH 7.5) and 250 mM NaCl and treated with a protease inhibitor cocktail. Further, the cells were lysed by sonicating at 40%

amplitude. The samples were centrifuged and syringe filtered using a 0.45 µm syringe filter. Purification was done by loading these in Ni-NTA chromatography (affinity chromatography). The protein was eluted with buffer containing 55 mM Tris-HCl, 250 mM NaCl, pH 7.5 at 10 mM and 250 mM imidazole. The purified protein was concentrated using a Pierce protein concentrator at a cutoff value of 10 kDa. Sephadex 75 pg gel filtration column (size exclusion-based chromatography) in an AKTA start purification system was adapted for further purification. The purified protein was run on 12% SDS-PAGE for visualization [2].

Biophysical characterization

Isothermal titration calorimetry

Thermodynamic parameters and binding affinity of SME-1 protein with vaborbactam & Taniborbactam were studied using Malvern ITC-PEAQ instrument at 25 ºC [3,4]. SME-1 protein and inhibitors were dissolved in phosphate buffer at pH 7.5. The sample cell was loaded with 280 µL protein (50 µM concentration), and the injection syringe was loaded with 40 µL inhibitor (concentration ranging from 400 µM to 700 µM). The protein-inhibitor interaction was studied over 19 injections, each of 2 µL inhibitor [5,6]. As Ledaborbactam is not soluble in water, DMSO was used as a cosolvent, but DMSO was creating a lot of noise in the ITC data; therefore, we did not include the ITC data of Ledaborbactam.

Biochemical characterization

Steady State Kinetics: Kinetic experiments

Enzyme inhibition profile was studied spectroscopically using a Cary 60 UV spectrophotometer. The hydrolysis of nitrocefin was monitored using a direct competition assay at steady-state conditions. The inhibition assay was performed at a fixed protein (10 nM) and nitrocefin (80 µM) concentration. The inhibitor concentration was varied from 0.1 to 10 µM in a total reaction volume of 1 ml for all 3 boronates. The instrument software was used to obtain the initial velocities and the absorbance vs time graph [7].

Equation 1 clearly depicts the inhibition mechanism of the inhibitors studied with SME-1 enzyme.

$$E + I \leftrightarrow E{:}I \leftrightarrow E - I \qquad \textbf{(1)}$$

The initial steady-state velocity, V_o, was plotted as $(1/V_o)$ vs inhibitor concentration to generate a Dixon plot. The apparent Ki (corrected) (Ki_{app}) was computed using this, and further observed Ki_{app} was corrected using equation 2.

$$Kiapp\ (corrected) = Kiapp\ (observed)/\{1 + ([S]/[KmNCF]\ )\} \qquad \textbf{(2)}$$

Where [S] was the concentration of nitrocefin (NCF). $Kiapp\ (corrected)$ is denoted as "ki" in the results section [8].

Borylation and deborylation

Borylation and deborylation rate was evaluated using nitrocefin as the reporter molecule for all three boronates. 100 µM of nitrocefin was dissolved in 50 mM sodium phosphate, pH 7.6, with 0.02% Tween-20. The reactions were monitored using BioTek SYNERGY H1 microplate reader at 30°C. For

borylation rate determination, 1 nM of SME-1 protein and 0.1 to 5 µM of the boronates (vaborbactam, taniborbactam, ledaborbactam) were used. The pseudo-first-order constant, kobs, was determined by fitting the progress curve to Equation 3 using GraphPad Prism 10.

$$P = Vs + (V0 - Vs)\frac{(1 - e^{-kt})}{k} \quad \textbf{(3)}$$

where, V_o was the uninhibited enzyme velocity that is measured in the absence of boronic acid in a reaction with SME-1 enzyme. V_s was the fully inhibited enzyme velocity, which was measured without the enzyme. The borylation efficiency (k_2/K_i) for SME-1 enzymes with both the isomers were determined by fitting the k_{obs} obtained with varied boronic acid concentrations to Equation 4 [8].

$$kobs = k - 2 + \frac{\frac{k2}{ki}|I|}{1 + \frac{|S|}{Km}} \quad \textbf{(4)}$$

To determine the deborylation rate (k_{-2}), a jump dilution assay was performed at room temperature. 1 µM of SME-enzyme was first treated with 10 µM of vaborbactam in 50 mM phosphate buffer (pH 7.6) with 0.02% Tween-20. After pre-incubation of 2 hours, the enzyme-inhibitor complex was diluted 100 times using the same buffer. The reaction was started by adding 180 µl of 200 µM nitrocefin to 20 µl of the diluted inactivation mixture [9]. The activity of nitrocefin hydrolysis by the enzyme was continuously recorded by measuring the absorbance at 486 nm (A486) using the microplate reader. This continuous assay monitored the regain of activity by SME-1. k_{-2} was obtained by fitting the progress curve to equation (4) using GraphPad Prism. For deborylation efficiency (k_{-2}) determination, V_0 was considered as the fully inhibited enzyme velocity, and V_S represented the uninhibited enzyme velocity [8]. Exactly the same procedure was used for Taniborbactam and Ledaborbactam.

Crystallization

Crystallization screening of SME-1 protein was performed using the sitting drop method. The crystallization screen was optimized by using 10 mg/ml purified protein in 96-well sitting drop plates (Art Robbins) using different crystallization screens such as PACT Premier, MIDAS Plus, LMB Screen (Molecular Dimensions), and Rigaku Wizard Screens [10]. The reservoir wells were filled with 70 µl of the crystallization conditions. Each drop was prepared by mixing equal volumes of protein and precipitate solution (0.8 µl each) onto the drop platform. To allow vapor equilibration, the plate was air-sealed and incubated at 20 ºC. The plates were monitored for crystal growth at regular intervals. Once the crystal condition was optimized, the crystal was improved by setting in hanging drop plates with a drop volume of 1to 3 uL [1,11,12].

Data collection & refinement

The complex of protein with vaborbactam, taniborbactam, and ledaborbactam was obtained by separately soaking pre-formed SME-1 crystals. Crystals were first grown in 20% PEG 4000 and 0.2 M Lithium Chloride crystal conditions and soaked with inhibitor solutions for 5 to 60 minutes. Following incubation, crystals were cryo-protected by a brief immersion in a solution containing 15% Xylitol in the mother liquor. X-ray diffraction data of SME complexes were collected using Rigaku Micromax

HF-007, having a Hypix detector and a rotating anode (Cu: 1.54 Å) source. The crystals mounted on the goniometer base were exposed to at least 30 seconds with a scan width of less than 0.20 degrees. The diffraction data were processed using Crysalis Pro and scaled with Aimless in the CCP4 i2 package. The initial structure was obtained by molecular replacement using CCP4 i2[13–16]. The resulting model was subjected to multiple rounds of manual model building and refinement using WinCoot. The coordinates and structure factors of the SME inhibitor complex have been submitted to the Protein Data Bank[1].

Biological Assay

Scanning electron microscopy

E. coli TOP10 cells transformed with the SME-1 plasmid vector and control cells were grown to mid-log phase, i.e., until O.D reached 0.6. 100 µl of aliquots were either treated with antibiotics alone, inhibitors + antibiotics or untreated control, and incubated overnight at 37ºC[17,18]. The cells were centrifuged at 6000 rpm for 5 minutes at 4 ºC and washed with sterile 0.1 M sodium phosphate buffer at pH 7.6. The pellets were further resuspended in the same buffer. A small volume of samples is placed on a coverslip and air-dried. Fixation was performed using glutaraldehyde in PBS solution for 1-2 hours. The fixed samples were dehydrated using a graded ethanol-water series, such as 30, 50, 70, 80, 90, 95, 100 % for 15-20 min each. The mounted samples were sputter-coated with a thin layer of gold. The effect of inhibitors on the bacterial cell morphology was visualized using Apreo S LoVac FESEM [7].

Antimicrobial Susceptibility Testing (AST)

The susceptibility of SME-1 gene-containing bacterial cells towards three boronates was determined by comparing the minimum inhibitory concentration performed using the broth dilution method. *E. coli* TOP10 cells transformed with the SME-1 plasmid vector were grown until the OD reached 0.6 and diluted to achieve 10^5 CFU/ml. With a starting concentration of 128 ug/ml, two-fold serial dilutions of the compounds in MH broth were prepared in the 96-well plate. 100 µl of bacterial cells were added to each well and incubated for 16-18 hours at 37ºC. MIC values were determined by visually scoring based on the turbidity [19].

Initial Structure Preparation

The initial three-dimensional coordinates of three systems, SME-1 and its covalently complexed with vaborbactam (PDB ID: 9W7N), taniborbactam (PDB ID: 9W7O), and ledaborbactam (PDB ID: 9W7P), were retrieved from experimentally determined X-ray crystallographic structures submitted to the Protein Data Bank. In all covalent complexes, the boronate-containing inhibitors were modelled as covalently bound to the catalytic Ser70 residue to reflect the acyl-enzyme intermediate state. The geometrical and conformational parameters of the boronate-containing inhibitors were optimized using the FFParam package [20] which automatically generates atom types and bonded parameters compatible with classical force fields. Crystallographic inconsistencies, such as missing side chains or alternate occupancies, were resolved through structural organisation using the CHARMM-GUI web interface [21]

Simulation Setup with Optimized Parameters

All molecular dynamics (MD) simulations were performed using GROMACS 2024.4 on a GPU-accelerated Linux cluster [22]. Each protein or protein-ligand complex was embedded in a cubic simulation box with a 1.0 nm buffer from the solute to the box edges, followed by solvation with explicit

TIP3P water molecules. Appropriate amounts of K^+ and Cl^- counterions were added to each system to balance its net charge and guarantee electrostatic neutrality [23].

Both bonded and non-bonded interactions were parameterized using the CHARMM36 all-atom force field[24]. The steepest descent algorithm was initially implemented to minimize energy when the maximum atomic force was lowered below 1,000 $kJmol^{-1}nm^{-1}$. This was followed by equilibration under isothermal-isobaric (NPT) conditions using the Berendsen thermostat ($\tau\_T = 0.1$ ps) and barostat ($\tau\_P = 0.2$ ps), with periodic boundary conditions applied in all directions [25]. All bonds involving hydrogen atoms were constrained using the LINCS algorithm, allowing for an integration time step of 2 fs. Long-range electrostatic interactions were treated using the Particle Mesh Ewald (PME) method [26] with a cutoff of 1.0 nm for both electrostatics and van der Waals forces [27]. Each system was subjected to a 500 ns production run, yielding a cumulative simulation time of 1.5 μs across the three systems.

Simulation Derived Trajectory Analysis

Post simulation trajectory analysis was performed using standard built-in GROMACS tools. Time-resolved structural stability was assessed via root-mean-square deviation (RMSD), local residue fluctuations via root-mean-square fluctuation (RMSF), global compactness via radius of gyration (Rg), solvent-exposed surface area (SASA), and time-dependent secondary structure profiles (B-factor analysis, snapshots) [28]. Visualization of protein dynamics, preparation of high-resolution figures and videos were carried out using PyMOL [29], OriginPro, Version 2025 [30] and UCSF Chimera [31].

References:

1 K. Dhankhar, G. Chakraborty, A. Bera, A. Chowdhary, A. Bandyopadhyay, N.-R. C. Mishra, N. Patra and S. Hazra, DOI:10.1101/2025.07.17.665329.

2 S. Bhattacharya, V. Junghare, N. K. Pandey, D. Ghosh, H. Patra and S. Hazra, *Int J Biol Macromol*, 2020, **145**, 510–526.

3 M. Bastos, O. Abian, C. M. Johnson, F. Ferreira-da-Silva, S. Vega, A. Jimenez-Alesanco, D. Ortega-Alarcon and A. Velazquez-Campoy, *Nature Reviews Methods Primers 2023 3:1*, 2023, **3**, 1–23.

4 J. M. Di Trani, S. De Cesco, R. O'Leary, J. Plescia, C. J. Do Nascimento, N. Moitessier and A. K. Mittermaier, *Nature Communications 2018 9:1*, 2018, **9**, 1–7.

5 S. Bhattacharya, A. K. Padhi, V. Junghare, N. Das, D. Ghosh, P. Roy, K. Y. J. Zhang and S. Hazra, *Int J Biol Macromol*, 2021, **177**, 337–350.

6 S. Bhattacharya, V. Junghare, N. K. Pandey, S. Baidya, H. Agarwal, N. Das, A. Banerjee, D. Ghosh, P. Roy, H. K. Patra and S. Hazra, *Front Microbiol*, DOI:10.3389/FMICB.2021.710291/FULL.

7 S. Bhattacharya, V. Junghare, M. Hazra, N. K. Pandey, A. Mukherjee, K. Dhankhar, N. Das, P. Roy, R. C. Dubey and S. Hazra, *ACS Bio and Med Chem Au*, DOI:10.1021/ACSBIOMEDCHEMAU.2C00044/SUPPL_FILE/BG2C00044_SI_002.AVI.

8 Z. Sun, H. Lin, L. Hu, N. Neetu, B. Sankaran, J. Wang, B. V. V. Prasad and T. Palzkill, *Journal of Biological Chemistry*,

DOI:10.1016/J.JBC.2023.105493/ATTACHMENT/E1E51A1D-D737-46E9-929F-5A6BCF6C0EA3/MMC1.DOCX.

9 A. Krajnc, J. Brem, P. Hinchliffe, K. Calvopiña, T. D. Panduwawala, P. A. Lang, J. J. A. G. Kamps, J. M. Tyrrell, E. Widlake, B. G. Saward, T. R. Walsh, J. Spencer and C. J. Schofield, *J Med Chem*, 2019, **62**, 8544–8556.

10 K. Dhankhar, S. Bhattacharya, M. Hazra, N. Pandey, N. Mishra, and S. Hazra, MDPI. 2025.

11 W. Sougakoff, G. L'Hermite, L. Pernot, T. Naas, V. Guillet, P. Nordmann, V. Jarlier and J. Delettré, *urn:issn:0907-4449*, 2002, **58**, 267–274.

12 W. Sougakoff, V. Jarlier, J. Delettré, N. Colloc'H, G. L'Hermite, P. Nordmann and T. Naas, *J Struct Biol*, 1996, **116**, 313–316.

13 L. Potterton, J. Agirre, C. Ballard, K. Cowtan, E. Dodson, P. R. Evans, H. T. Jenkins, R. Keegan, E. Krissinel, K. Stevenson, A. Lebedev, S. J. Mcnicholas, R. A. Nicholls, M. Noble, N. S. Pannu, C. Roth, G. Sheldrick, P. Skubak, J. Turkenburg, V. Uski, F. Von Delft, D. Waterman, K. Wilson, M. Winn and M. Wojdyr, *journals.iucr.org*, DOI:10.1107/S2059798317016035.

14 R. N.-A. C. S. D. S. Biology and undefined 2017, *journals.iucr.org*.

15 M. A. Hough and K. S. Wilson, *Acta Crystallogr D Struct Biol*, 2018, **74**, 67.

16 M. Hough, K. W.-A. crystallographica. S. D and undefined 2018, *ncbi.nlm.nih.gov*.

17 C. Le Terrier, V. Gruenig, C. Fournier, P. Nordmann and L. Poirel, *Lancet Infect Dis*, 2023, **23**, 401–402.

18 H. Feng, J. Ding, D. Zhu, X. Liu, X. Xu, Y. Zhang, S. Zang, D. C. Wang and W. Liu, *J Am Chem Soc*, 2014, **136**, 14694–14697.

19 A. Mukherjee, J. Barman, C. Ghosh, R. Adhikary, K. Dhankhar, P. Roy, S. Basu and S. Hazra, *ACS Infect Dis*, 2025, **11**, 653–664.

20 A. Kumar and A. D. MacKerell, *Journal of Physical Chemistry B*, 2024, **128**, 4385–4395.

21 L. Kong, S. J. Park and W. Im, *J Mol Biol*, 2024, **436**, 168554.

22 J. A. Lemkul, *J Phys Chem B*, 2024, **128**, 9418–9435.

23 I. V. Leontyev and A. A. Stuchebrukhov, *J Chem Theory Comput*, 2012, **8**, 3207–3216.

24 J. Huang, S. Rauscher, G. Nawrocki, T. Ran, M. Feig, B. L. De Groot, H. Grubmüller and A. D. MacKerell, *Nature Methods 2016 14:1*, 2016, **14**, 71–73.

25 M. Dobson, *Journal of Chemical Physics*, DOI:10.1063/1.4901276/15487673/184103_1_ACCEPTED_MANUSCRIPT.PDF.

26 B. Hess, *J Chem Theory Comput*, 2008, **4**, 116–122.

27 T. Darden, L. Perera, L. Li and P. Lee, *Structure*, 1999, **7**, R55–R60.

28 D. Van Der Spoel, E. Lindahl, B. Hess, G. Groenhof, A. E. Mark and H. J. C. Berendsen, *J Comput Chem*, 2005, **26**, 1701–1718.

29 PyMOL | www.pymol.org, https://www.pymol.org/pymol.html?, (accessed 14 May 2025).

30 OriginLab - Origin and OriginPro - Data Analysis and Graphing Software, https://www.originlab.com/, (accessed 6 August 2025).

31 E. F. Pettersen, T. D. Goddard, C. C. Huang, G. S. Couch, D. M. Greenblatt, E. C. Meng and T. E. Ferrin, *J Comput Chem*, 2004, **25**, 1605–1612.